Elastic scattering of ^{84}Kr by ^{208}Pb†

R. Vandenbosch and M. P. Webb
University of Washington, Seattle, Washington 98195

T. D. Thomas
Oregon State University, Corvallis, Oregon 97331

S. W. Yates* and A. M. Friedman
Argonne National Laboratory, Argonne, Illinois 60439
(Received 29 September 1975)

Angular distributions for the elastic scattering of ^{84}Kr by ^{208}Pb at 494, 510, and 718 MeV have been measured. Fresnel, parametrized phase shift, and optical model analyses show that Coulomb deflection and surface absorption effects dominate. The optical model analysis shows that the results are sensitive to the nuclear potential only in the vicinity of the strong absorption radius, giving a value of the nuclear potential at this distance that is in agreement with a number of theoretical estimates.

[NUCLEAR REACTIONS ^{208}Pb(^{84}Kr, ^{84}Kr), E = 494, 510, and 718 MeV; measured $\sigma(\theta)$; Fresnel, parametrized phase shift and optical model analyses.]

I. INTRODUCTION

The interaction of very heavy projectiles with heavy targets appears to be considerably different from that exhibited in lighter systems.[1-3] Not only is the probability for complete fusion of a heavy target nucleus with a heavy projectile quite small, but also the direct processes, which comrise the bulk of the reaction cross section, can be very inelastic. In order to understand these features it is important to know the effective potential between the target and projectile and also to know the integrated cross section for absorption from the elastic channel. We have therefore measured the elastic scattering of ^{84}Kr by ^{208}Pb at energies close to the barrier and at the highest available energy. The results are analyzed in terms of Fresnel scattering, parametrized phase shift analysis, sharp cutoff, and optical models. Interaction radii and absorption cross sections are deduced from these models.

II. EXPERIMENTAL

The ^{84}Kr beam was obtained from the Super-HILAC (heavy ion linear accelerator) of the Lawrence Berkeley Laboratory. The general experimental setup has been described elsewhere.[4] The beam exhibited an energy resolution of approximately 1% under the conditions of this experiment. Some structure in the beam was observed with two components separated by several MeV often being present. Periodic checks of the beam energy were made during the course of the measurements, and the data reported were taken under conditions where the beam energy did not vary by more than about 1%. The absolute energy of the beam is believed to be accurate to within 1.5%. The beam was collimated to 0.32 cm diameter yielding particle currents of 1–2 nA. The target was 50 μg/cm^2 thick ^{208}Pb, 99.14% isotopically pure. The elastically scattered particles were detected by movable surface barrier solid state detectors subtending a solid angle of 1.4 msr with an angular acceptance of 0.75° (lab) in the reaction plane. A third, fixed-position, detector served as a monitor. Suppression of electrons from the targets was effected by a combination of biasing the target, covering the detectors with a thin Ni foil, and placing a magnetic field in the path between the detectors and the target.

The elastic peak typically exhibited an energy width of 8–10 MeV full width at half maximum. A kinematic spread of 2.4 MeV was expected from the finite angular acceptance of the detector. The spread in energy associated with energy loss in the target was approximately 0.6 MeV. The remaining width is due to contributions from the finite detector resolution and the energy spread of the beam, mostly the latter. The integration of the elastic peak typically included events within 15 MeV of the most probable energy. Thus, the "elastic" peak includes some contributions from inelastic scattering and transfer reactions with small Q values. Absolute cross sections were obtained by normalizing the observed for-

ward-angle elastic scattering to Rutherford scattering.

III. RESULTS AND DISCUSSION

The elastic scattering angular distributions, plotted as the ratio of the elastic cross section to Rutherford scattering, are shown in Fig. 1. They exhibit an initial rise above unity followed by a smooth and near-exponential descent at larger angles. These features are characteristic of the elastic scattering for systems with large values of the Sommerfeld parameter, $\eta = Z_1 Z_2 e^2/\hbar v$. The results at $E_{lab} = 494$ MeV are similar to the results at $E_{lab} = 500$ MeV reported by Colombani *et al.*,[5] except that the present results do not exhibit as large a rise above unity. This disagreement probably reflects the fact that track detectors with poorer energy discrimination were used in the previous experiment and allowed a less complete separation of elastic and nonelastic events.

The differences between the elastic scattering at the two energies are primarily a consequence of the dependence of the Coulomb deflection on the trajectory of the projectile. This can be illustrated by plotting the ratio of elastic and Rutherford cross sections as a function of the distance of closest approach

$$d = Z_1 Z_2 e^2 / 2 E_{c.m.} [1 + \csc(\tfrac{1}{2}\theta)]$$

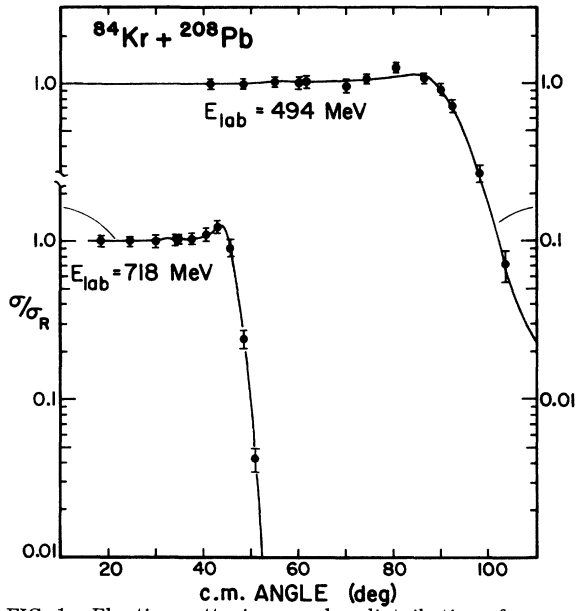

FIG. 1. Elastic scattering angular distributions for (a) 494 MeV and (b) 718 MeV ^{84}Kr ions scattered by ^{208}Pb. The full curves are optical model fits to the data. The curve for 494 MeV is from the $V = 50$ potential of Table II, while the curve for 718 MeV is from a potential with $V = 50$, $r_V = 1.129$, $a_V = 1.1$, $W = 32$, $r_W = 1.211$, and $a_W = 0.43$.

for Coulomb trajectories. Such a plot is shown in Fig. 2. In this representation the falloff of the elastic cross section from Rutherford scattering is seen to occur at very nearly the same distance of closest approach at both bombarding energies.

A. Sharp cutoff model analysis

In the sharp cutoff model[6] all partial waves with angular momentum below the critical angular momentum l_c are assumed to be absorbed. For partial waves with l larger than l_c only the Coulomb potential affects the trajectory. The cutoff value for the angular momentum is given by $l_c = \eta \cot(\frac{1}{2}\theta_c)$, where θ_c is the center-of-mass angle at which the ratio of the elastic cross section to the Rutherford cross section is 0.25. The sharp-cutoff radius is given by

$$R_c = \frac{Z_1 Z_2 e^2}{2E_{c.m.}} [1 + \csc(\tfrac{1}{2}\theta_c)]$$

from which the radius parameter $r_{0c} = R_c/(A_1^{1/3} + A_2^{1/3})$ is obtained. The absorption cross section is given by $\sigma = \pi R_c^2 (1 - V/E)$, where V is the value of the Coulomb potential at $R = R_c$. The values obtained for these parameters from the data shown in Figs. 1 and 2 are presented in Table I. Also listed are values obtained from a less complete data set for $E_{lab} = 510$ MeV. The values of R_{0c} are smaller than observed in reactions induced by lighter projectiles, but are consistent with a trend for sharp cutoff r_{0c} values to decrease with increasing mass numer of the projectile. This dependence can be attributed[7,8] to the diffuseness of the nuclear surface, which is

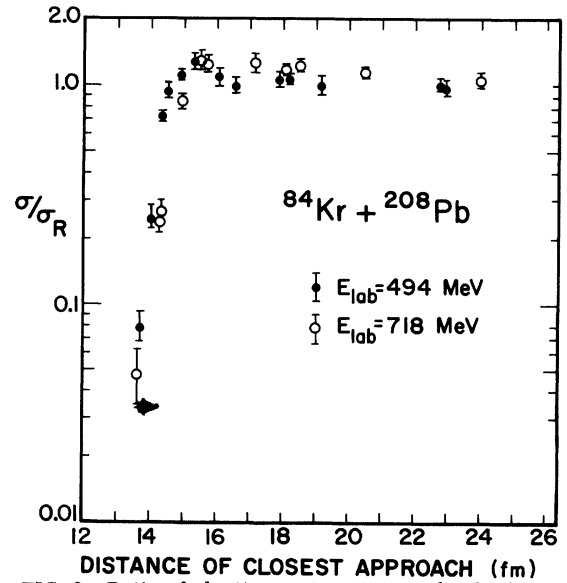

FIG. 2. Ratio of elastic scattering to Rutherford scattering as a function of the distance of closest approach for Coulomb trajectories.

TABLE I. Sharp cutoff model parameters.

Incident laboratory energy (MeV)	θ_c (deg)	l_c	R_c	r_{0c}	σ_{abs}
494	98	166.6	14.04	1.36	865
510	89	192	14.2	1.38	1115
718	48.5	353	14.27	1.386	2670

a relatively smaller fraction of the interaction distance as the size of projectile and/or target increase. In Table I distances are in fm, σ is in mb.

B. Optical model analysis

The elastic scattering has been analyzed using two optical model codes[9] especially developed for very heavy ion scattering. Up to 1000 partial waves were employed because of the large values of kR encountered. In order to save computer time in some preliminary calculations the scattering amplitudes were calculated only for every other partial wave and these values were used to interpolate for the remaining partial waves. It was also possible to assume that the lowest 100 or so partial waves were completely absorbed in preliminary calculations. A search routine[10] was also employed and this routine had the possibility of utilizing these time-saving features. It was found rather soon that it was impossible to adequately fit the angular distributions with

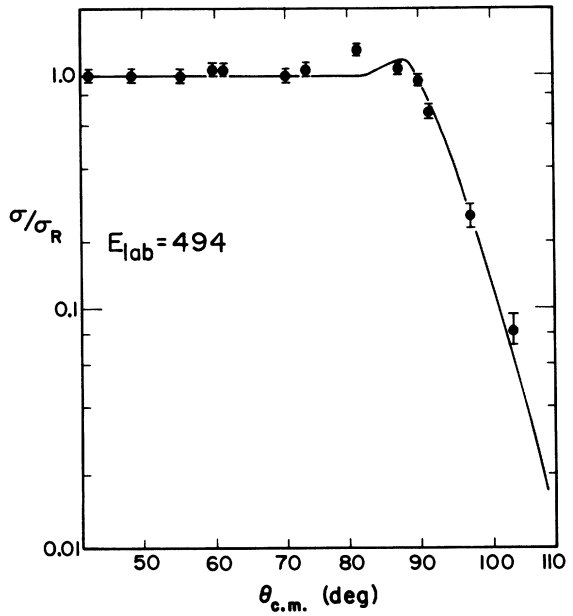

FIG. 3. Comparison of elastic scattering data with an optical model fit under the restraint of common geometry for the real and imaginary potentials. The parameters are $V=27.75$, $W=26.2$, $r_V=r_W=1.334$, $a_V=a_W=0.125$, and originate from a potential of Huizenga *et al.* (Ref.11).

potentials where the real and imaginary potential had the same geometry. When attempts were made to do so, potentials that gave the correct large-angle falloff always predicted a rise in σ/σ_R at too large an angle. This effect is illustrated in Fig. 3, using a potential found in a search starting with a potential[11] used in the ^{209}Bi $+^{84}$Kr system at 600 MeV. In order to qualitatively reproduce the broad rise in σ/σ_R at the correct angle it is necessary to use a nuclear potential that exhibits surface transparency. This feature of the data may arise in part from our failure to completely separate the quasielastic events from the true elastic events. There is, however, considerable evidence for the necessity of surface transparency in other heavy ion systems. Surface transparent potentials have been employed for some time in describing the elastic scattering of such systems as ^{16}O+^{16}O and have also been found to be necessary to account for interference effects observed in transfer reactions on medium mass targets.[12] Surface transparency was achieved in the present situation by making the imaginary potential less diffuse than the real potential. Examples of optical model fits to the data are shown in Fig. 1. The fact that the geometry of the potentials is somewhat different at the two energies is not surprising in that the l dependence is expected to change with bombarding energy[13] and the present potentials simulate l dependence by having different geometries for the real and imaginary potential.

Although the imaginary part of the surface-transparent potential has a fairly sharp surface associated with the small diffuseness, the localization in l space of the absorption is not very sharp. The transmission coefficients $T_l=(1-|\eta_l|^2)$ for the potential used in the fit to the 494 MeV data are shown in Fig. 4, where it is seen that the T_l values fall from 0.9 to 0.1 between l values of 130 and 184.

We have not made extensive explorations of potential ambiguities because of the computational time involved. We have made some calculations at $E_{lab}=494$ where the imaginary potential and the Coulomb potential were held fixed and only the real potential parameters were varied. The imaginary potential found in the $V=50$ potential was used in this exploration. It was found that real potentials satisfying the Igo ambiguity ($Ve^{R/a}=$const) did not give equivalent fits under the restraint of a fixed imaginary and Coulomb potential. Moderately satisfactory fits under these conditions could be obtained at other V values by adjusting the real potential radius and diffuseness parameters, r_v and a_v. Slight adjustments in the imaginary potential restored the fits close to their

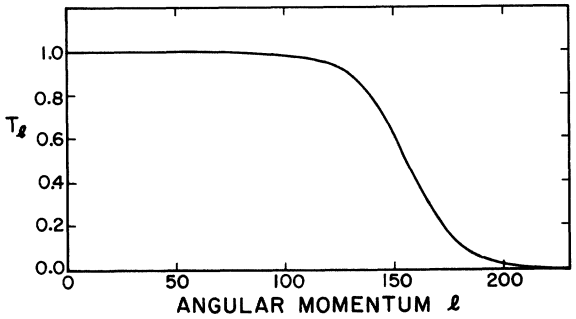

FIG. 4. Transmission coefficients as a function of angular momentum for the optical potential used in Fig. 1(a).

original quality. Some of these results are summarized in Table II.

The reaction cross section in the optical model analysis is given by $\sigma = \pi\lambda^{-2}\sum_l (2l+1)T_l$, where T_l is the transmission coefficient of the lth wave. The values calculated with the optical model of 885 mb at 494 MeV and 2509 mb at 718 MeV, are consistent with those found by use of the sharp cutoff model (see Table I).

Although the radii and diffuseness of the potentials with different depths varied greatly, it was found that all of the real potentials associated with a fixed imaginary potential became essentially the same at a particular value of the separation R, as can be seen in Fig. 5. An additional ambiguity in the determination of the real potential is introduced when the imaginary potential is allowed to vary independently. An extreme example of this is illustrated in Fig. 6, where a very shallow real potential associated with a different imaginary potential is compared with the envelope of the potentials of Fig. 5. We also show here a real potential obtained in the fit to the 718 MeV data, and also a potential where the real and imaginary potentials were restrained to have the same geom-

TABLE II. Study of potential ambiguities in fits to elastic scattering at 494 MeV. The first set of potentials uses the imaginary potential found with $V=50$ and only r_V and a_V were optimized. For the second set the imaginary potential was varied also at each V.

V	r_V	a_V	W	r_W	a_W	χ^2	Strong [a] absorption radius (fm)
300	0.895	1.48	2.5	1.282	0.33	1.88	14.2
100	1.06	1.247	2.5	1.282	0.33	1.55	
50	1.178	1.1	2.5	1.282	0.33	0.87	
25	1.293	0.78	2.5	1.282	0.33	1.11	
10	No satisfactory real potential found with this imaginary potential						
100	1.058	1.255	2.45	1.281	0.346	1.38	13.8
50	1.178	1.1	2.5	1.282	0.33	0.87	
25	1.292	0.785	2.7	1.282	0.33	0.90	
10	1.345	0.505	2.1	1.353	0.2	1.0	

[a] The strong absorption radius given here is obtained from the expression $L(L+1) - kR(kR - 2\eta)$ where $\eta = Z_1 Z_2 e^2/\hbar v$ and L is the orbital angular momentum for which the absolute value of the reflection coefficient is 0.5.

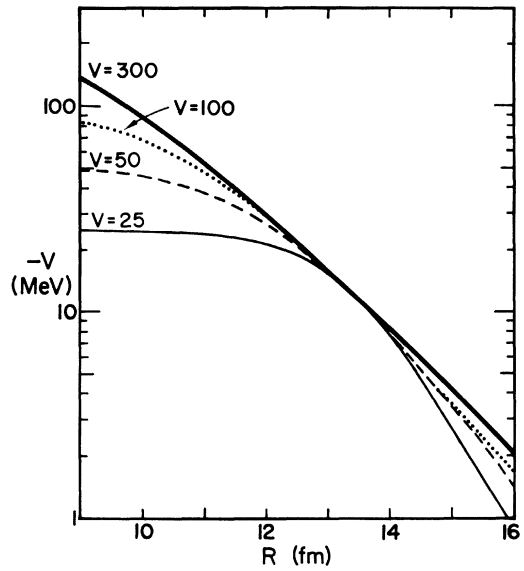

FIG. 5. Comparison of real nuclear potentials obtained in the fit to the 494 MeV data under the restraint of a fixed imaginary potential. The complete specification of the potentials is given in the top part of Table I.

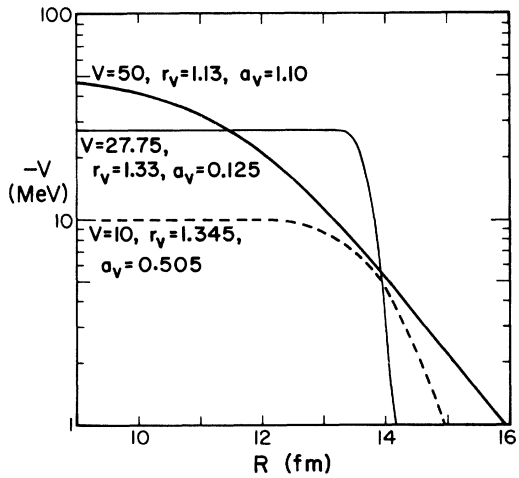

FIG. 6. Comparison of some widely different real potentials. The $V=10$ MeV potential is a shallow potential that fits the $E_{lab}=494$ MeV data. The $V=27.75$ potential was obtained under the restraint of a common geometry for the real and imaginary potential (see caption to Fig. 3). The $V=50$ potential is based on a fit to our $E_{lab}=718$ MeV data.

etry. This latter potential does not give as good a fit to the scattering data, but again one sees that as the best potential with this restraint it gives about the same value of V at $R = 14$ as the other potentials. We conclude that analysis of elastic scattering enables determination of the magnitude and the slope of the potential for R values only in the vicinity of $R = 14$ fm. This distance is about equal to the strong absorption radii determined from theoretical models[14] and with the sharp cutoff model listed in Tables I and II. A similar conclusion has been reached by Garrett *et al.*[15] in an analysis of the elastic scattering of ^{32}S by ^{27}Al by Satchler in an analysis of a variety of heavy ion reactions,[16] and by Glendenning.[17]

The nuclear potential in the region where it can be determined from elastic scattering measurements is compared with a number of theoretical or empirical potentials in Fig. 7. The curve labeled Ngô *et al.*[18,19] is based on a calculation by the method proposed by Brueckner *et al.*[20] using nuclear matter densities given by Beiner and Lombard.[21] The curve labeled "Proximity potential" is taken from the work of Randrup, Swiatecki, and Tsang.[22] It is based on a theorem relating the force between two undeformable gently curved objects in close proximity to the interaction potential between flat surfaces. The functional form of the latter has been calculated using an effective momentum-dependent nucleon-nucleon force and the nuclear Thomas-Fermi approximation. The numerical evaluation is based on the surface energy coefficient of Myers and Swiatecki.[23] A more recent version[24] of the proximity formula (which uses experimental surface diffusivities rather than the slightly underestimated values given by the Thomas-Fermi method) results in values of the potential between $R = 12$ and 14 fm which are almost indistinguishable from the curve labeled Ngô *et al.* The curve labeled "Krappe-Nix" is a generalization[25] of the sharp-surface liquid drop surface energy by folding over short-range two-particle interaction of the Yukawa type. All of these potentials are in quite good agreement with the potential determined from the elastic scattering measurements. Becuase of the insensitivity of elastic scattering to distances very far from the strong absorption it will be very difficult to discriminate between the various potentials.

C. Fresnel and parametrized phase shift analyses

The data at 494 MeV were also analyzed in terms of Fresnel[26] scattering and the parametrized phase shift model.[14] The results are in relatively

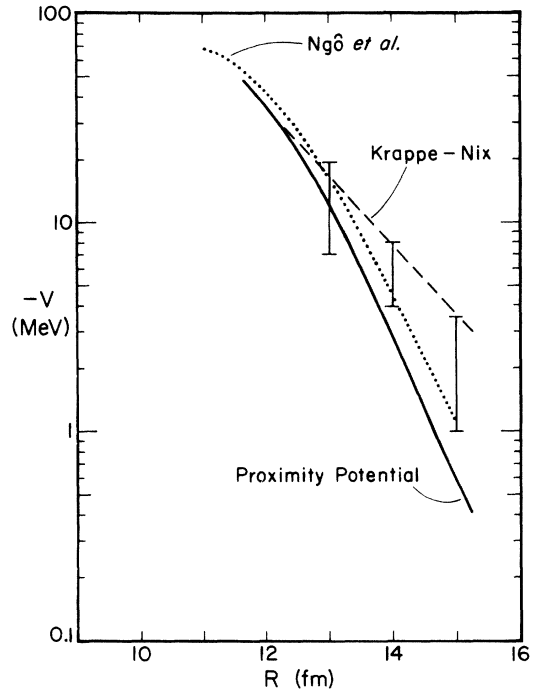

FIG. 7. Comparison of nuclear potential obtained in this work from analysis of elastic scattering with theoretical or empirical potentials appearing in the literature.

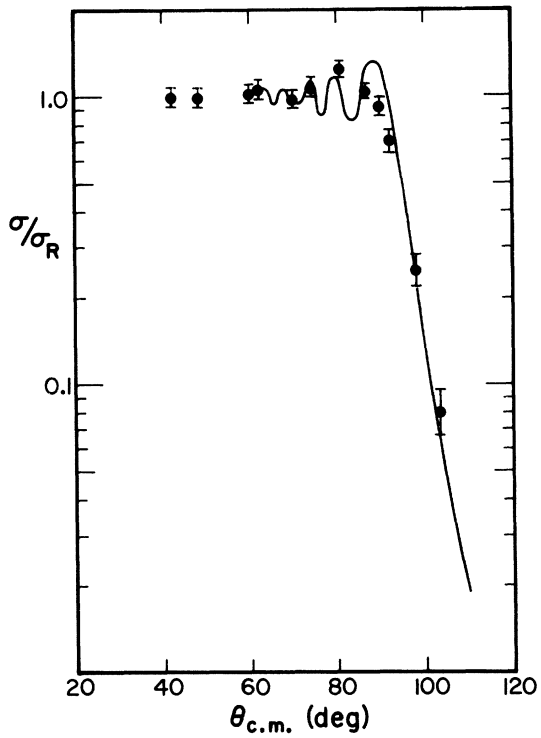

FIG. 8. Comparison of elastic scattering data at $E_{lab} = 494$ MeV with the Fresnel scattering pattern for $l_c = 166$.

good agreement with the other analyses. A comparison of the 494 MeV data with the Fresnel pattern is shown in Fig. 8. The slope of the falloff of the experimental values of σ/σ_R is very close to that predicted by Fresnel scattering. The extracted total reaction cross sections were 780 and 760 mb for the Fresnel and phase shift analyses, respectively. The strong absorption radii were found to be 14.0 and 13.6 fm for the two respective cases. However, since neither of these models include details of the potential between projectile and nucleus we will not consider them more closely. The results of these two analyses do confirm the qualitative features of the results of the more model-dependent calculations.

IV. SUMMARY

The analysis of the elastic scattering data at 494 and 718 MeV indicate that the observed effects are dominated by Coulomb deflection and absorption at the nuclear surface. The fact that the ratio σ/σ_R is the same function of the Rutherford distance of approach at both energies, as shown in Fig. 2, tends to confirm this description of the process. The rate of falloff of σ/σ_R at large angles is close to that given by Fresnel scattering. In addition, the fact that all equally useful optical potential sets agree only at the strong absorption radius shows that only these surface interactions are important in determining the elastic scattering.

The total reaction cross sections found by use of all models are about 1000 mb at 500 MeV and about 2500 mb at 718 MeV. However, as is well known, the total fusion cross sections[27,4] in this region have been found to have an upper limit of 50 mb at 500 MeV and 800 mb at 718 MeV. This may either be related to entrance channel effects or to the fact that the effective fission barrier is expected to be zero for the high Z^2/A compound nucleus that would be formed.[4]

ACKNOWLEDGMENTS

We are indebted to Richard Eppley for assisting us in preparing for experiments at the Super-HILAC and Yuen-dat Chan for providing the search routine used in the optical model calculations. We also want to thank Dr. J. C. Jacmart and Dr. P. Colombani for communicating their experimental data on krypton scattering.

---

†Work supported in part by the U. S. Energy Research and Development Administration.

*Present address: University of Kentucky, Lexington, Kentucky 40506.

[1]F. Hanappe, M. Lefort, C. Ngô, J. Peter, and B. Tamain, Phys. Rev. Lett. 32, 738 (1974).

[2]A. G. Artukh, G. F. Gridnev, V. L. Mikheev, V. V. Volkov, and J. Wilczynski, Nucl. Phys. A215, 91 (1973).

[3]M. Lefort, C. Ngô, J. Péter, and B. Tamain, Nucl. Phys. A216, 166 (1973).

[4]R. Vandenbosch, M. P. Webb, and T. D. Thomas (unpublished).

[5]P. Colombani, J. C. Jacmart, N. Poffé, M. Riou, C. Stephan, and J. Tys, Phys. Lett. 42B, 197 (1972).

[6]J. S. Blair, Phys. Rev. 95, 1218 (1954).

[7]J. M. Alexander, H. Delagrange, and A. Fleury, Phys. Rev. C 12, 149 (1975).

[8]C. Y. Wong, Phys. Lett. 42B, 186 (1972); T. D. Thomas, Phys. Rev. 116, 703 (1959).

[9]At Argonne a modified version of ABACUS was used. At the University of Washington a modified version (designated HOP-THREE) of the code HOP-TWO was used.

[10]Search routine SCHOMP, written by Yuen-dat Chan, University of Washington.

[11]J. R. Huizenga, in Proceedings of the Meeting of the American Chemical Society, April 7, 1975, Philadelphia, Pennsylvania (unpublished).

[12]M. J. Levine, A. J. Baltz, P. D. Bond, J. P. Garrett, S. Kahana, and C. E. Thorn, Phys. Rev. C 10, 1602 (1974).

[13]R. W. Shaw, Jr., R. Vandenbosch, and M. K. Mehta, Phys. Rev. Lett. 25, 457 (1970).

[14]A. M. Friedman, R. H. Siemssen, and J. G. Cuninghame, Phys. Rev. C 6 2219 (1972).

[15]J. D. Garrett, H. E. Wegner, T. M. Cormier, E. R. Cosman, O. Hansen, and A. J. Lazzarini (unpublished).

[16]G. R. Satchler, in *Proceedings of the International Conference on Reactions Between Complex Nuclei, Nashville, Tennessee, 1974,* Vol. 2, edited by R. L. Robinson, F. K. McGowan, and J. B. Ball, (North-Holland, Amsterdam/American Elsevier, New York, 1974), Vol. 2, p. 171.

[17]N. K. Glendenning, Rev. Mod. Phys. 47, 659 (1975).

[18]C. Ngô, B. Tamain, J. Galin, M. Beiner, and R. J. Lombard, Nucl. Phys. A240, 353 (1975).

[19]We are indebted to Professor Marc Lefort for sending us the numerical values of the Kr potential calculated by Galin, Ngô, and Lefort.

[20]K. A. Brueckner, J. R. Buchler, G. Jorna, and R. J. Lombard, Phys. Rev. 171, 1188 (1968); 181, 1543 (1969).

[21]R. J. Lombard and M. Beiner, in *Proceedings of the International Conference on Nuclear Physics, Munich, 1973,* edited by J. de Boer and H. J. Mang (North-Holland, Amsterdam/American Elsevier, New York, 1973), Vol. II, p. 39; M. Beiner and R. J. Lombard, Ann. Phys. (N.Y.) 86, 262 (1974).

[22]J. Randrup, W. J. Swiatecki, and C. F. Tsang, Lawrence Berkeley Laboratory Report No. LBL-3606 (unpublished).

[23]W. D. Myers and W. J. Swiatecki, Ark. Fys. 36, 343 (1967).

[24]W. J. Swiatecki, Lawrence Berkeley Laboratory Report

No. LBL-4296 (unpublished).
[25]H. J. Krappe and J. R. Nix, in *Proceedings of the Third International Atomic Energy Symposium on Physics and Chemistry of Fission, Rochester, 1973* (IAEA, Vienna, 1974).
[26]W. H. Frahn, Nucl. Phys. 75, 577 (1966).
[27]M. Lefort, C. Ngô, J. Pêter, and B. Tamain, Nucl. Phys. A216, 166 (1973).